Epitaxial growth and structural property of graphene on Pt(111)

M. Gao, Y. Pan, L. Huang, H. Hu, L. Z. Zhang, H. M. Guo, S. X. Du, and H.-J. Gao[a)]
Institute of Physics, Chinese Academy of Sciences, P.O. Box 603, Beijing 100190, People's Republic of China

(Received 14 December 2010; accepted 27 December 2010; published online 18 January 2011)

We report on epitaxial growth of graphene on Pt(111) surface. It was found out that the proportion of different rotational domains varies with growth temperature and the graphene quality can be improved by adjusting both the growth temperature and ethylene exposure. Rippled and unrippled domains of high quality graphene are observed. The adhesive energy and electronic structure of two models, representing rippled and unrippled graphene, are obtained with density functional theory calculation, which shows that the interaction between graphene and Pt(111) surface is very weak and the electronic structure is nearly the same as that of a free standing graphene. © *2011 American Institute of Physics*. [doi:10.1063/1.3543624]

The discovery of exfoliated graphene in 2004 (Ref. 1) started an upsurge of researches in preparations,[2–5] properties,[6–9] and applications[10,11] of the material. This brought epitaxial graphite films on SiC (Ref. 4) and transition metal surfaces into the focus of interest further again,[12–16] which were usually prepared by segregation of bulk-dissolved carbon onto surfaces or chemical decomposition of hydrocarbons. Recently, high quality epitaxial monolayer graphite films (referred as epitaxial graphene or EG in the following) were reported on transition metal surfaces, such as Ru(0001),[17] Ir(111),[18] Cu(111),[19,20] and Ni thin film.[21] The growth mechanism of EG on Ru(0001) and Ir(111) has been investigated by low energy electron microscopy and scanning tunneling microscopy (STM).[22,23] A nonlinear kinetic growth model of graphene on Ru(0001) was established based on the analysis of graphene growth rates as a function of adatom concentration, and thus a cluster-addition mechanism was suggested. [24] It is also observed that the growth temperature can drastically affect the quality of graphene on Ir(111).[22] On the other hand, Pt(111) substrate is of distinctive interests because the Pt substrate has the minimum affect on the physical properties of graphene due to very weak graphene-substrate interaction. However, less work was conducted on the growth of different graphene domains on Pt(111) and its formation mechanism.

In this letter, we report that at about 800 K with an ethylene exposure of 37.6 L the quality of graphene on Pt(111) gets improved due to sparse nucleation. We changed the growth temperature and ethylene exposure and investigated the quality of EG by low energy electron diffraction (LEED) and STM. Combining STM with density functional theory (DFT) calculation, the geometric and electronic structure of the graphene was also studied.

The experiment was carried out in an ultrahigh vacuum (UHV) chamber with the base pressure lower than 1×10^{-10} mbar. The chamber is equipped with a room temperature STM, an Auger electron spectroscopy (AES), a LEED, and an electron beam heating (EBH) stage. The Pt substrate is a commercial product whose (111) surface has been polished to less than 0.03 μm of roughness. It was cleaned by several cycles of ultrasonic cleaning in high purity acetone and ethanol to remove the organic contamination on the surface. Then the crystal was loaded into the UHV chamber and cleaned by cycles of 0.6 keV Ar+ sputtering followed by annealing to high temperature till the AES spectra showing no contaminations. Graphene was prepared by exposing the Pt(111) substrate to high purity (99.995%) ethylene while the substrate temperature was varied from 773 to 1073 K. The temperature was measured by a tungsten-rhenium (W–5%Re/W–26%Re) thermocouple welded to the EBH stage. The formation of graphene on Pt(111) was confirmed by carbon peak at 272 eV in AES spectrum.

The growth temperature has great influence on the structure and quality of graphene layer grown on metal substrates. Therefore the growth of EG was studied at different substrate temperature with the fixed exposure of ethylene to Pt(111). The partial pressure of ethylene was 5×10^{-7} mbar and the exposure lasted 100 s. Figure 1 shows the evolution process of LEED patterns of the graphene layer with increasing substrate temperature: (a) 773 K, (b) 873 K, and (c) 973 K, respectively. The six sharp spots come from Pt(111) substrate, corresponding to the sixfold symmetrical structure. The outer arc shape spots are from EG layers. At lower growth temperature, the center of arc shape spots are rotated by an angle of 19° relative to the sharp spots from Pt, as shown in Figs. 1(a) and 1(b). The diffraction spots of EG obtained at 873 K are shorter and brighter than those at 773 K, indicating an increase in the R19° domains. When the temperature increases to 973 K [Fig. 1(c)], the center of the arc shape spots are rotated by an angle of 30° relative to the spots from Pt, and faint spots in line with the Pt spot appears.

The LEED results show much information of the relation between growth temperature and rotation angles. First, there are three kinds of main rotation angles, 0°, 19°, and 30°, respectively, which corresponding the possible rotation angles between graphene lattice and Pt(111) surface lattice.

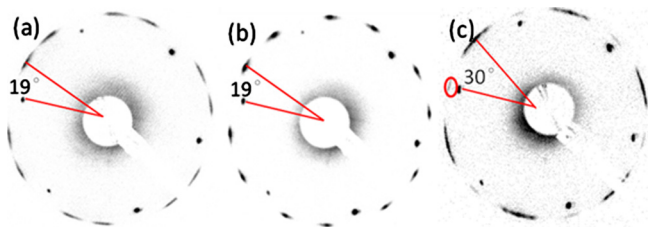

FIG. 1. (Color online) LEED pattern of EG on Pt (111) prepared by exposing to ethylene at different temperature, (a) 773, (b) 873, and (c) 973 K. The beam energy is 60 eV.

[a)]Electronic mail: hjgao@iphy.ac.cn.

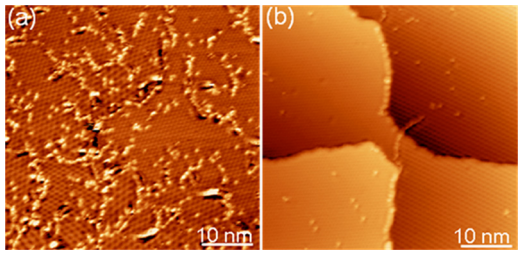

FIG. 2. (Color online) STM images of graphene grown on Pt (111) (V_s =0.04 V, I=1.5 nA). (a) For an exposure of 376 L at 1073 K, the domain size is small; (b) For an exposure of 37.6 L at 773 K, the domain size is much bigger than that in (a).

Arc shape spots instead of round spots are observed from LEED pattern of graphene layer, indicating the graphene locally ordered but with varying orientation in different domains. Second, the proportion of different rotational domains is dependent on the growth temperature. It had been reported that supersonic methane molecules with a higher kinetic energy can induce highly oriented monolayer graphite on Pt(111).[25] However, our results show that at very high temperature the arc shape spots are still observable, indicating multiple domains of graphene are unavoidable on Pt(111). The formation of various structures of graphene layers on Pt(111) surface is mainly attributed to the modulated energy barrier of attaching carbon atoms to the different orientation of graphene edge during the epitaxial growth process.[22]

Since the orientation of graphene domains varies no matter what the growth temperature is, the quality of EG, i.e., domain size and crystallization, can only be improved by reducing the density of nuclei at early stage and the density of defects while growing.[26] In order to study the effort of ethylene exposure and growth temperature on the quality of EG, we use STM to probe the EG in real space. Figure 2(a) shows a STM image of EG prepared at an exposure of 376 L (5×10^{-6} mbar for 100 s) at 1073 K. The domain boundaries and defects result in the corrugation of graphene and show bright spots in STM images. The domains size is very small (several to tens of nanometers), and the density of defects on the domain is very high. However, EG with large domain size (more than one hundred of nanometers) are observed on a sample prepared at an exposure of 37.6 L (5×10^{-7} mbar for 100 s) at 773 K, as shown in Fig. 2(b). This is because at high temperature and large exposure, the density of surface carbon is very high and thus dense nucleation occurs. To improve the quality of EG on Pt(111), one need to carefully control the temperature and exposure to keep the surface carbon concentration not far above the limit of nucleation, so that the sparse nucleation of graphene is achieved. Also, the growth speed is low at lower surface carbon concentration, thus the density of defects can be reduced.

The hexagonal moiré superstructure comes from superposition of graphene honeycomb lattice and Pt hexagonal lattice underneath. Its orientation and periodicity varies with the rotation angle between the two lattices in each domain, as the examples given Fig. 3 and Table I. According to its orientation with respect to graphene lattice, two categories of moiré superstructures are found. In the first category, the lattice vectors of moiré superstructures are parallel to the lattice vector of graphene, as in 2×2, 3×3, and 4×4 domains shown in Figs. 3(a)–3(c), respectively. The height profile across the dashed green lines in each STM image is plotted in Fig. 3(g). The corrugation of these domains is within 0.03 nm, indicating the graphene film is very flat without much distortion in vertical direction. In the second category, there are angles between the lattice vectors of moiré superstructures and graphene, as in the ($\sqrt{37}\times\sqrt{37}$) R21°, ($\sqrt{61}\times\sqrt{61}$) R26°, and ($\sqrt{67}\times\sqrt{67}$) R12° domains shown in Figs. 3(e)–3(g). The corrugation of these domains increased to 0.05–0.08 nm, as can be seen in Fig. 3(h), more like the rippled graphene on Ir(111) and Ru(0001) with fluctuated bonding strength with the substrate.[17,18] The corrugation difference originates from the different rotation angles of each domain with respect to the Pt substrate, as given in the last column of Table I. The domains in the second category rotated a very small angle, as a result the carbon atom within a supercell coordinate with the substrate differently because of the lattice mismatch, just like the case of graphene on Ru and Ir; while the domains in the first category rotated a lot, resulting similar coordination with the

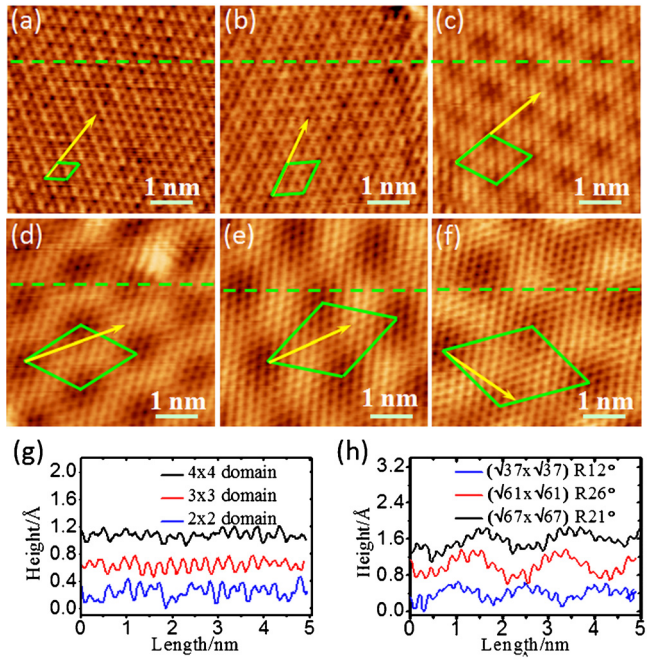

FIG. 3. (Color online) Atomic resolution STM image of six rotational domains with different moiré supercell with respect to primary graphene lattice (V_s=−0.4 V, I=0.2 nA): (a) 2×2, (b) 3×3, (c) 4×4, (d) ($\sqrt{37}\times\sqrt{37}$) R21°, (e) ($\sqrt{61}\times\sqrt{61}$) R26°, and (f) ($\sqrt{67}\times\sqrt{67}$) R12°. The $\langle 2\bar{1}\bar{1}0\rangle$ direction of graphene lattices is indicated by the yellow arrows and moiré unit cells are in green rhombus. The height profiles along the green dashed lines in each image are plotted in (g) and (h).

TABLE I. The periodicity of each moiré superstructure in Fig. 3 and corresponding rotation angles between graphene and Pt lattices.

Figure	Moiré superstructure with respect to graphene	Moiré periodicity (nm)	The rotation angle between graphene and Pt lattices (°)
Figure 3(a)	2×2	0.5	30
Figure 3(b)	3×3	0.738	19
Figure 3(c)	4×4	1	14
Figure 3(d)	($\sqrt{37}\times\sqrt{37}$) R21°	1.5	6
Figure 3(e)	($\sqrt{61}\times\sqrt{61}$) R26°	1.87	3
Figure 3(f)	($\sqrt{67}\times\sqrt{67}$) R12°	2.1	2

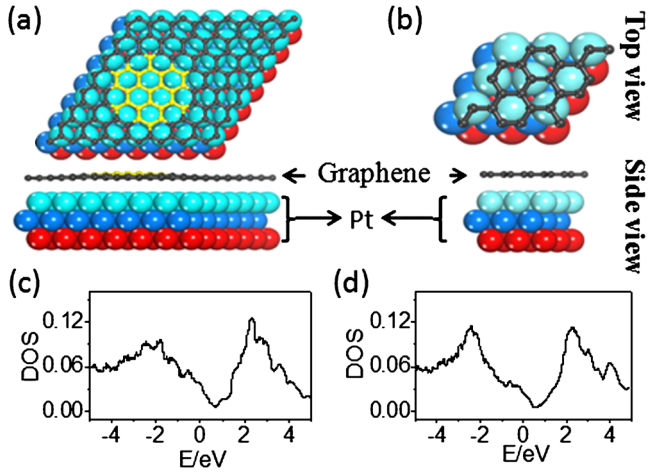

FIG. 4. (Color online) Two models of monolayer graphene on Pt(111). (a) A model constructed by putting 8×8 graphene unit cells on 7×7 unit cells of Pt(111), representing rippled graphene on Pt(111). (b) A model of 2×2 supercell, the same as the moiré pattern in Fig. 3(a), representing unrippled graphene. (c) and (d) are the calculated DOS curves for model (a) and (b), respectively.

substrate for each carbon atoms in a supercell. Nevertheless, the different corrugations imply different physical nature at the interfaces.

To get a better understanding of the properties of EG on Pt(111) surface, we used DFT based first principle calculation to investigate its geometric structure and electronic structure. Two structural models were built to represent the rippled and unrippled graphene in each category discussed before. The thickness of Pt substrate was tested, and the results show that three Pt layers were adequate to simulate the system. For the first one, the graphene lattice vectors are aligned along the Pt(111) lattice with no rotation. A 8×8 supercell is used, which means 7×7 Pt(111) lattices matching 8×8 graphene lattices, as shown in Fig. 4(a), to represent the highly rippled graphene. The calculation results show the corrugation of graphene is 0.053 nm in this model, which is consistence with our STM results. In the second model, to construct the structure in which the graphene lattice has a rotation angle of 30° with respect to the Pt(111) lattice [Fig. 3(a)], a special supercell is built to represent the unrippled graphene, as shown in Fig. 4(b). It has the minimum stress and the smallest supercell structure.

The calculated average adhesive energies of per carbon atom are 38.6 meV and 39.8 meV for the two models shown in Figs. 4(a) and 4(b), respectively, implying that the interaction between graphene and Pt(111) surface is really small. Therefore various EG domains with different orientations could coexist at high temperature. In addition, the optimized structures shows that the graphene layers have an interfacial distance of more than 0.31 nm with the Pt(111) surface due to the weak graphene-substrate interaction, which is much larger than that on Ni(111) and Ru(0001) surface[27] that have strong interaction with graphene. These calculation results also confirmed that the interaction between graphene and the substrate is very weak. The local density of states (LDOS) of the graphene on Pt(111) surface were also calculated. As shown in Figs. 4(c) and 4(d), the LDOS of graphene remains "V" shape, indicating that due to the weak interaction, the electronic structure of graphene is nearly unaffected by Pt(111) surface. The up-shift of the Dirac point is induced by the a little charge transfer from graphene to Pt(111) surface.

In summary, we have grown epitaxially the monolayer graphene on Pt(111) surface by chemical decomposition of ethylene. The quality of EG is improved by achieving sparse nucleation at proper growth temperature and ethylene exposure. DFT calculation result shows that the interaction between graphene and Pt(111) surface is very weak and the electronic structure is nearly the same as that of free standing graphene.

This project was supported by grants from the NSFC, National "973" project of China, and the CAS.

[1]K. S. Novoselov, A. K. Geim, S. V. Morozov, D. Jiang, Y. Zhang, S. V. Dubonos, I. V. Grigorieva, and A. A. Firsov, Science **306**, 666 (2004).
[2]S. Stankovich, D. A. Dikin, G. H. B. Dommett, K. M. Kohlhaas, E. J. Zimney, E. A. Stach, R. D. Piner, S. T. Nguyen, and R. S. Ruoff, Nature (London) **442**, 282 (2006).
[3]K. S. Kim, Y. Zhao, H. Jang, S. Y. Lee, J. M. Kim, K. S. Kim, J. H. Ahn, P. Kim, J. Y. Choi, and B. H. Hong, Nature (London) **457**, 706 (2009).
[4]C. Berger, Z. M. Song, X. B. Li, X. S. Wu, N. Brown, C. Naud, D. Mayo, T. B. Li, J. Hass, A. N. Marchenkov, E. H. Conrad, P. N. First, and W. A. de Heer, Science **312**, 1191 (2006).
[5]Y. Pan, D.-X. Shi, and H.-J. Gao, Chin. Phys. **16**, 3151 (2007).
[6]Y. B. Zhang, Y. W. Tan, H. L. Stormer, and P. Kim, Nature (London) **438**, 201 (2005).
[7]N. Tombros, C. Jozsa, M. Popinciuc, H. T. Jonkman, and B. J. van Wees, Nature (London) **448**, 571 (2007).
[8]A. K. Geim and K. S. Novoselov, Nature Mater. **6**, 183 (2007).
[9]K. S. Novoselov, Z. Jiang, Y. Zhang, S. V. Morozov, H. L. Stormer, U. Zeitler, J. C. Maan, G. S. Boebinger, P. Kim, and A. K. Geim, Science **315**, 1379 (2007).
[10]J. S. Bunch, A. M. van der Zande, S. S. Verbridge, I. W. Frank, D. M. Tanenbaum, J. M. Parpia, H. G. Craighead, and P. L. McEuen, Science **315**, 490 (2007).
[11]P. K. Ang, W. Chen, T. S. W. Andrew, and K. P. Loh, J. Am. Chem. Soc. **130**, 14392 (2008).
[12]A. T. N'Diaye, S. Bleikamp, P. J. Feibelman, and T. Michely, Phys. Rev. Lett. **97**, 215501 (2006).
[13]J. Coraux, A. T. N'Diaye, C. Busse, and T. Michely, Nano Lett. **8**, 565 (2008).
[14]D. Martoccia, P. R. Willmott, T. Brugger, M. Bjorck, S. Gunther, C. M. Schleputz, A. Cervellino, S. A. Pauli, B. D. Patterson, S. Marchini, J. Wintterlin, W. Moritz, and T. Greber, Phys. Rev. Lett. **101**, 126102 (2008).
[15]P. W. Sutter, J. I. Flege, and E. A. S. Er, Nature Mater. **7**, 406 (2008).
[16]Y. S. Dedkov, M. Fonin, U. Rudiger, and C. Laubschat, Phys. Rev. Lett. **100**, 107602 (2008).
[17]Y. Pan, H. G. Zhang, D. X. Shi, J. T. Sun, S. X. Du, F. Liu, and H. J. Gao, Adv. Mater. **21**, 2777 (2009).
[18]A. T. N'Diaye, J. Coraux, T. N. Plasa, C. Busse, and T. Michely, New J. Phys. **10**, 043033 (2008).
[19]X. S. Li, W. W. Cai, J. H. An, S. Kim, J. Nah, D. X. Yang, R. Piner, A. Velamakanni, I. Jung, E. Tutuc, S. K. Banerjee, L. Colombo, and R. S. Ruoff, Science **324**, 1312 (2009).
[20]L. Gao, J. R. Guest, and N. P. Guisinger, Nano Lett. **10**, 3512 (2010).
[21]T. Iwasaki, H. J. Park, M. Konuma, D. S. Lee, J. H. Smet, and U. Starke, Nano Lett. **11**, 79 (2011).
[22]E. Loginova, N. C. Bartelt, P. J. Feibelman, and K. F. McCarty, New J. Phys. **11**, 063046 (2009).
[23]J. Coraux, A. T. N'Diaye, M. Engler, C. Busse, D. Wall, N. Buckanie, F. Heringdorf, R. van Gastei, B. Poelsema, and T. Michely, New J. Phys. **11**, 023006 (2009).
[24]E. Loginova, N. C. Bartelt, P. J. Feibelman, and K. F. McCarty, New J. Phys. **10**, 093026 (2008).
[25]H. Ueta, M. Saida, C. Nakai, Y. Yamada, M. Sasaki, and S. Yamamoto, Surf. Sci. **560**, 183 (2004).
[26]P. Sutter, J. T. Sadowski, and E. Sutter, Phys. Rev. B **80**, 245411 (2009).
[27]M. Gao, Y. Pan, C. D. Zhang, H. Hu, R. Yang, H. L. Lu, J. M. Cai, S. X. Du, F. Liu, and H. J. Gao, Appl. Phys. Lett. **96**, 053109 (2010).